Effective substrate emissivity during dew water condensation

Joachim Trosseille, Anne Mongruel, Laurent Royon, Daniel Beysens

Effective substrate emissivity during dew water condensation

Joachim Trosseille[a,*], Anne Mongruel[a], Laurent Royon[b], Daniel Beysens[a,c]

[a] *Physique et Mécanique des Milieux Hétérogènes, CNRS, ESPCI Paris - PSL University, Sorbonne Université, Sorbonne Paris Cité, 75005, Paris, France*
[b] *Laboratoire des Energies de Demain, Sorbonne Paris Cité, UMR 8236CNRS, 75013, Paris, France*
[c] *OPUR, 2 rue Verderet, 75016 Paris, France*

Abstract

Dew formation is due to the radiative cooling of a surface. Surface emissivity is classically considered without the contribution of water condensation. However the latter, with an emissivity of ϵ_w=0.98, can occupy more than 80% of the surface and strongly affect is radiative properties. Here we present experimental and theoretical studies of the effective surface emissivity, taking into account the presence of the condensing water. The main results are concerned with the effect of the dry surface emissivity on condensation. On the one hand it appears that there is a significant difference between high and low emissivity substrates in the duration of a transient regime at the begining of condensation, making the overall condensation yield smaller for low emissivity substrates. On the other hand, in permanent regime of condensation, the effective surface emissivity is dominated by the presence of drops and the condensation only weakly depends on the dry surface emissivity. These results are of practical importance and can be extended to all application involving radiative heat transfer with condensation.

Keywords: Dew, Condensation, Radiative cooling, Emissivity

2010 MSC: 00-01, 99-00

*Corresponding author
Email address: joachim.trosseille@espci.fr (Joachim Trosseille)

1. Introduction

Dew is ubiquitous in nature. Its formation involves the cooling of a substrate (plant, soil or artificial substrate) below the dew point temperature of the surrounding humid air. Such a process is ensured by the radiation deficit between the substrate and the atmosphere and is, as a consequence, thought to be all the more efficient that the substrate emissivity is close to unity. As a matter of fact, most of dew condensation studies assume for radiative exchange a substrate emissivity without condensed water [1, 2, 3, 4]. It appears, however, that condensation alters this picture as the presence of water droplets should modify the emissivity of the substrate according to the surface coverage of the droplet pattern. One interesting measurement was reported by Maestro-Valero et al. [5] concerning the spectral emissivity of dry and wet plastic substrate. They showed by spectral measurements that substrate emissivity in the 7-14 μm band was increased when wet. Unfortunately, they did not characterize further this effect nor what were the wet conditions.

Figure 1 shows a thermal map of drops (darker spots) condensed on a reflective substrate (brighter spots). As explained in section 3.2, each color correspond to a different value of emissivity. The darker is the color, the higher is the emissivity. The different zones (A,B,C,D), explicited in section 5.1, highlight the non-homogeneity and the diversity of emissivity pattern on a condensing surface. At a local scale, emissivity depends strongly on the presence of water on a specific point and only affects the local energy balance. At a larger scale, the global energy balance of a condensing surface depends on what we call effective emissivity, which takes into account the coverage of water on the surface. For practical reasons (heat transfer calculations, condensation rates, etc...), the global energy balance is more often preferred, which requires the knowledge of the interplay between water surface coverage and surface effective emissivity.

It is therefore the object of this study to investigate quantitatively the effect of condensation on surface effective emissivity during condensation. For this purpose we use two substrates with small and large emissivities while show-

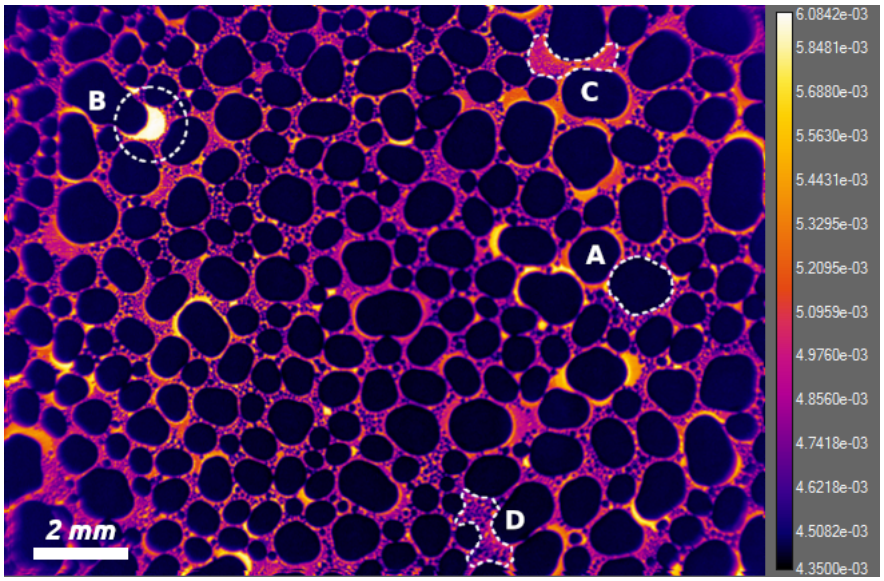

Figure 1: Close up view of droplets condensed on a reflective substrate($\varepsilon_{S-} = 0.05$) . HR=62%, T_a=27°C, T_s=7.6°C. t=4000 s. A, B, C, D : zones of interest (see text). Color bar : mesured radiance ($W.m^{-2}.sr^{-1}$)

ing the same wetting properties. A specially designed experimental setup is used to create a radiative deficit between the substrate and a cold source, under controlled air temperature and humidity [6]. An infra-red camera is used to measure emissivity of the samples in the [7.5-14] μm range, the so-called atmospheric window where atmosphere is nearly transparent to IR radiations [7].

2. Drop surface coverage

The surface coverage of dew or breath figures pattern during dropwise condensation is defined as $e_d = \sum \pi R_i^2/S$ where R_i is the individual drop radius and S the area of the considered surface. It evolves during condensation following different stages of growth, this evolution depending only on the drops and substrate dimensionalities [8]. For diffusion limited condensation and for the general case of 3D droplets condensing on a 2D substrate, the different stages

are the following:

(i) Nucleation of droplets on substrate inhomogeneities.

(ii) Individual droplet growth with time t as $R_i \sim t^{1/2}$ when e_d is low, followed by a growth in $t^{1/3}$,

(iii) Self-similar growth when drops start to coalesce with each other. Individual drops grow as $R_i \sim t^{1/3}$ between coalescences, while the mean pattern radius evolves as $< R > \sim t$. The surface coverage e_d reaches there a limit e_d^0 due to the balance between drop growth, which increases e_d, and drop coalescence, which lowers e_d. The value of e_d^0 depends on the substrate wetting properties (drop contact angle θ) [9], as

$$e_d^0 \approx 1 - \frac{\theta(deg.)}{180} \tag{1}$$

(iv) Late stages, characterized by the re-nucleation of new droplet patterns on the bare surface between large drops with large interdistances (see zone D in figure 1 for instance), leading to the increase of the global surface water coverage. When p different drop patterns that have nucleated at p different times coexist (see [10] and Fig. 1, zones B, C, D)), one gets

$$e_d \approx 1 - (1 - e_d^0)^p \tag{2}$$

(v) Gravity makes the drops above a critical radius to slide down [11] and limits the drop sizes.

Note that one has to differenciate between e_d, the drop surface coverage of the substrate corresponding to the footprint of the drop on the substrate (dotted line in figure 2), from e_e, the projected drop surface coverage as seen from above (full line in figure 2). The relevant quantity to consider for radiative exchanges is e_e as defined by

$$e_e = \begin{cases} e_d & if \quad \theta < 90^\circ \\ 0.5 & if \quad \theta > 90^\circ \end{cases} \tag{3}$$

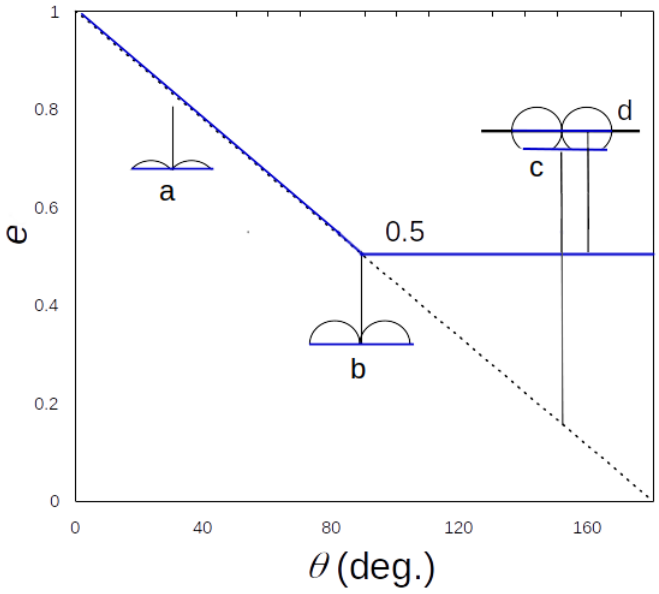

Figure 2: Variation with respect to the drop contact angle θ of surface and surface view coverages in the initial self-similar stage. Wet surface coverage e_d: Dotted line, cases a, b, c. Drop view surface e_e: Full lines a, b, d. (Adapted from [8] and [9])

3. Experiments and methods

In contrast with usual condensation experiments where cooling is ensured by contact, radiative condensation experiments requires some specific devices and materials. Samples are elaborated to provide materials with various emissivities but same wetting properties. An infrared camera is used to measure local and mean emissivities. Water condensation is performed in both radiative and conductive cooling devices.

3.1. Samples

Two samples of low and high emissivities but with same wetting properties are prepared in the following way. Thin sheets of different materials are prepared, with the same 6 μm thick transparent low density polyethylene (LDPE) sheet on top of each stack (figure 3). The monochromatic light transmission coefficient τ_λ of a thick transparent media can be calculated from equations 6

and 7 below using the extinction coefficient k_λ, *i.e.* the complex part of the refractive index of the material. Datas from [12] show that for LDPE in the wavelength range [1-20] μm the extinction coefficient is constant at $k \sim 10^{-3}$. Equations 6 and 7 can thus be used for integrated values and we get $\tau \simeq 0.99$ for a 6 μm thick film. The top LPDE thin sheet is thus highly transparent to IR and each composite material will present the same contact angle with water drops while having emissivity values depending on the material layers stacked under the first sheet.

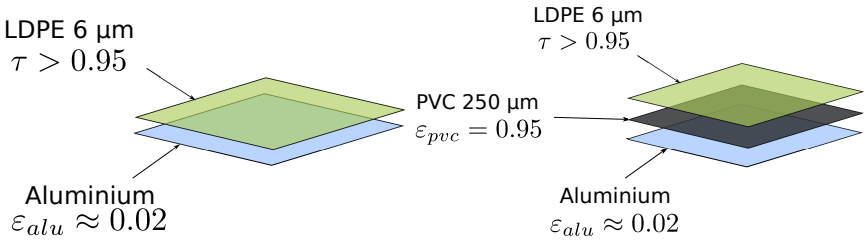

Figure 3: Stacks of different emissivities but same wetting properties (LDPE : low density polyethylene). Left: S- substrate ($\varepsilon_{S-} = 0.05$), Right: S+ substrate ($\varepsilon_{S+} = 0.88$). Other notations : see text.

Emissivities of samples are measured with an IR camera by the same technique as described in Section 3.2. The first sample, S-, is a stack of aluminium (emissivity $\varepsilon_{alu} \simeq 0.04$ [13]) and polyethylene sheets. The latter being highly transparent, the overall emissivity of the sample will be close to the emissivity of aluminium. In fact the emissivity of S-, measured by the same technique as explained in section 3.2 is $\varepsilon_{S-} = 0.05 \pm 0.05$. The second sample, S+, is 250 μm thick PVC sheet of emissivity $\varepsilon_{PVC} = 0.95$ [14] sandwiched between an aluminium sheet and the same polyethylene sheet above. As for S- the resulting emissivity of sample S+ will be close to the emissivity of the PVC sheet. As a result the overall emissivity of S+, measured as explained in section 3.2, is $\varepsilon_{S+} = 0.88 \pm 0.01$.

As the contact angle of water varies between its advancing (θ_a) and receding (θ_r) values due to drop coalescences, we choose to use an overall contact angle θ_m to characterise the wettability of the samples. The latter is calculated

from eq. 1, which relates the contact angle to the experimental measure of the surface coverage during the self-similar regime of condensation [9]. From the analysis of IR images (see fig. 1 at t=4000 s concerning the permanent regime of condensation) we get e_e^0=e_d^0=0.63 $\pm$ 0.02 and θ_m = 65.9° $\pm$ 3.6° for water on low density polyethylene.

3.2. Emissivity measurements

In order to measure the emissivity of the samples, we use a cooling device made out of a Peltier element homogenized by a thick electrolytic copper plate. The sample is stuck on the free surface of the Peltier stage which acts as a cold source. A contact cooling is thus used, as opposed to dew condensation which uses radiative cooling of the substrate. However, the emissivities as obtained from this method will be the same as gained with radiative cooling because the spatial properties of the condensation pattern, which are directly linked to the effective emissivity (see section 1), do not depend on the cooling process but only on the dimensionality of the droplets and the dimensionality of the substrate (see Ref.[8]). Experiments are performed at room temperature T_a=26°C and relative humidity (ratio of ambiant vapour pressure to the saturation pressure at ambiant temperature) RH = 48 %. The power of the Peltier element is adjusted in order to induce or avoid, depending on the experiment, condensation on the sample.

Emissivity measurements are made by means of a FLIR A655SC infra-red camera in the range [7.5-14] μm. The sensor of the camera is a 640x480px wide uncooled microbolometer. A 25 μm close-up lens is used to provide a spatial resolution of 42.8 px/mm at working distance. The IR camera does not perform direct emissivity measurements but measures the total radiance L_m received by each pixel of the sensor. The latter comes from (i) the radiance emitted by the object $\varepsilon L^0(T)$ with ε the emissivity of the object and $L^0(T)$ the radiance of a black body at same object temperature T in the range [7.5-14] μm, and (ii) the radiance reflected by the object from the ambient environment, $(1-\varepsilon)L^0(T_a)$. Here $L^0(T_a)$ is the radiance emitted by a black body at the temperature T_a of

the ambient environment in the range [7.5-14] μm. In this expression the atmosphere between the sensor and the object is considered transparent to infrared radiations considering the small distance between object and camera (< 0.5 m) and the spectral range of the camera [15, 16] . It thus follows

$$L_m = \varepsilon L^0(T) + (1-\varepsilon)L^0(T_a) \tag{4}$$

Equation 4 then gives access to the emissivity :

$$\varepsilon = \frac{L_m - L^0(T_a)}{L^0(T) - L^0(T_a)} \tag{5}$$

The measurement being performed on each pixel of the sensor, the radiance can then be averaged on a specific area. If one assumes that temperature is uniform on the surface, equation 5 gives a mean value of the emissivity on the area. As radiance measurements are performed between 7.5 and 14 μm, all values of measured emissivity in the manuscript will be total emissivity between 7.5 and 14 μm.

Two kinds of measurements are performed. The first measurement is the determination of the dry sample emissivity while the second measurement is a determination of the effective emissivity of the sample under condensation.

3.3. Condensation by radiative cooling

The substrate has to be cooled below the dew point temperature, that is the saturation temperature of a humid air at a given water vapor pressure. For that purpose, we use the same radiative cooling setup as described in [6] and hereafter denoted as "radiative chamber". Figure 4 reports its main features. The device is based on radiative interactions between a cold source (1) and the object (2) under study. An infrared heat transfer takes place between the cold source and the object. The object (2) is settled on a sample holder (3) weighed by a precision balance to monitor the evolution of the condensed mass. The object and sample holder are enclosed in a cylindrical container in which is injected humid air at relative humidity RH = 95 %. A set of mirrors (6) is

positioned around the object to intensify the radiative transfer with the cold source. The IR exchange is made through an IR transparent double window (5) separating the object from the cold source. Air flow at room temperature is sent between the two layers of the double window to avoid condensation on the IR transparent windows. Other windows (7-8) are present for visualization. Three thermocouples (T1, T2, T3) are placed in the chamber to monitor temperature during the experiments.

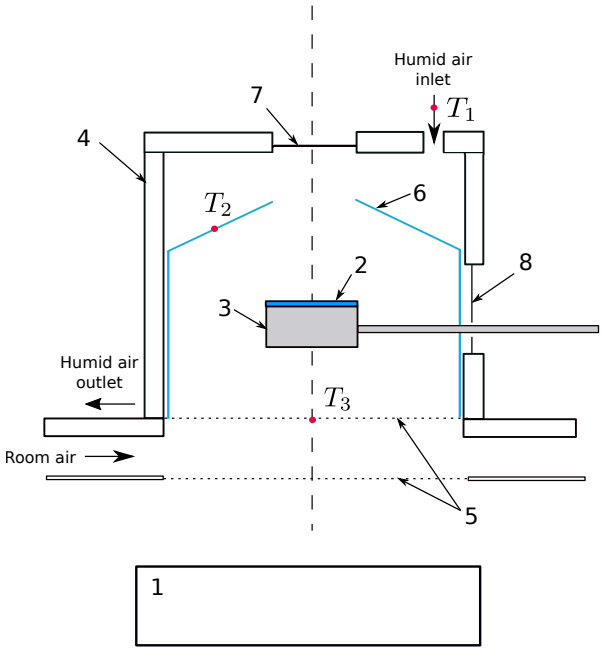

Figure 4: Schematics of the experimental setup. 1: Cold source ; 2: Cooled object ; 3: Stand ; 4: Cylindrical humid chamber; 5: IR - transparent window; 6: Mirrors ; 7-8: Visualization windows; arrows: Flow direction . T_1,T_2,T_3 : Thermocouples. (figure not to scale)

4. Results

For each sample described in section 3.1, two seprate experiments are carried out. In one experiment, the experimental setup described in section 3.2 is used. The sample is cooled by conduction and condensation is observed with an IR camera, in order to determine the evolution of the effective emissivity

of the condensing surface during the first times of condensation. In a second experiment, the sample is introduced into the radiative chamber described in section 3.3. The condensed mass of water is recorded in order to measure the dynamics of condensation by radiative cooling.

4.1. Effective emissivity evolution

The condensation is obtained by conductive cooling using a Peltier element, as noted in Section 3.2. The evolution of the radiance coming from the condensing surface is observed by IR camera.

Figure 5 shows a close-up view of the evolution of condensation on substrate S- (ε_{S-}=0.05) with RH = 62 %, an air temperature of T_a=27°C. After a transient regime between t=0 s ($T_c(t=0)$ =18.5°C) and t=1000 s in which temperature rapidly decreases under the action of the Peltier element, convection and heat release due to condensation compensate the cooling power. A thermal equilibrium is then reached after t=1000 s when the substrate temperature is T_c=7.6°C. At t=0 s, no drops are present on the substrate. Radiance received by the camera is high as light mainly comes from the reflection of the ambient radiation (factor $1-\varepsilon = 0.95$). Then radiance progressively diminishes (t=1000 s), corresponding to the nucleation of water drops on the substrate, which modify the local emissivity. At t=2000 s circular spots of lower radiance appear on the substrate, corresponding to condensed drops following the classical evolution discussed in Section 1, with a pattern showing regions of various radiances. These regions thus correspond to different local emissivities. This pattern then lasts until the end of the experiment, characterized by a self-similar growth of the droplets.

In order to examine the evolution of radiance and emissivity on substrates S- and S+ we use a larger view to take into account more drops and have a better statistics. Experiments are performed on substrates S- and S+ in the same thermal and humid air conditions, that is a relative humidity of RH = 48 %, an air temperature of T_a=26°C (yet slightly different from those of fig 5). As well as for the previous experiment, temperature decreases from $T_c(t=0)$ =16°C at

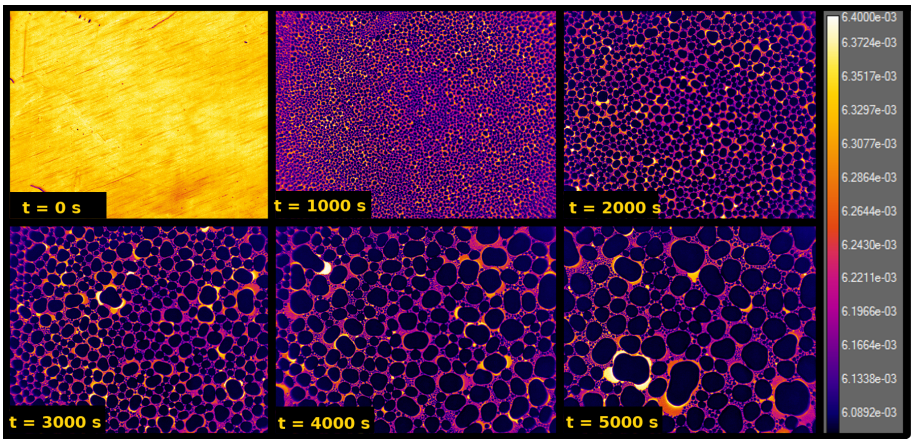

Figure 5: Repartition of radiance received by IR camera sensor in the [7.5-14] μm range from substrate S- during condensation . RH=62 %, T_a=27°C, T_c=7.6°C. Color bar : mesured radiance ($W.m^{-2}.sr^{-1}$)

t = 0s to T_c=7.6°C after t=1000 s under the action of the Peltier element.

Figure 6a shows the radiance map received by the thermal camera from surface S- (emissivity ε=0.05) during condensation. As well as described in the previous experiment, shown in figure 5, the radiance received by the camera decreases as drops condense on the surface, replacing part of the low emissivity dry surface by the emissivity of the drops. Figure 6b shows the radiance map received by the thermal camera from surface S- (emissivity ε=0.88). As opposed to the experiment on S-, the received radiance at t=0 s is low and mainly comes from the emission of the substrate. As condensation occurs on the surface, little modification of the received radiance is observed, despite condensation (same surface temperature and same material as for figure 6a.), attested by slight spots of lower radiance visible after t=5000 s.

Figure 7 shows the evolution of the mean effective emissivities calculated from equation 5 using the measured radiance shown in figure 6 averaged on the substrate area ($\approx$ 500 mm^2). Curve S- corresponds to the effective condensation emissivity on substrate S- and curve S+ on substrate S+. Curve W represents the emissivity ε_w = 0.98 of an infinitely thick layer of water (opaque, τ_w=0)

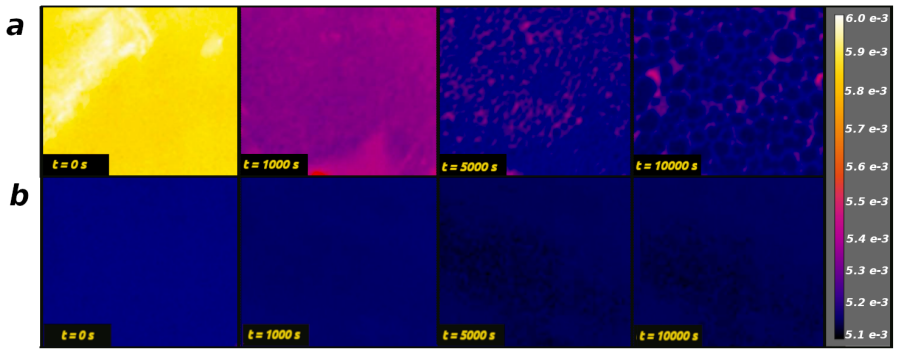

Figure 6: Repartition of radiance received by IR camera sensor in the [7.5-14] μm range from substrate S- (top) and S+ (bottom) during condensation . RH=48 %, T_a=26°C, T_c=7.6°C. Mean substrate emissivity varies from 0.05 at t=0 s to 0.87 at t=10000 s for S- and from 0.88 at t=0 s to 0.95 at t=10000 s for S+ (see Fig. 7). Field of view : 15x12.5 mm^2. After about 1000 s, S- and S+ emissivities become of comparable magnitude (see also Fig. 7). Color bar : mesured radiance ($W.m^{-2}.sr^{-1}$)

between 7.5 and 14 microns and curves S_0-,+ represents the dry substrate emissivities. Both curves S+ and S- show similar evolution. At t=0 s curve S- exhibits a value ε_{S-} ≈0.03, close to the emissivity of the dry substrate (0.05). Curve S+ shows the value $\varepsilon_{S+} \approx 0.87$, close to the emissivity of dry substrate (0.88). The slight decrease at very short time is due to the sharp temperature drop at the beginning of the experiment. In fact as temperature T drops, black body radiation at T and measured radiation (resp. $L^0(T)$ and L_{mes} in eq.5) decrease. The measured radiation decrease is however slowered by the dynamic of droplets condensation on the substrate which modifies the surface emissivity while growing. Measured radiation thus decreases slower than black body radiation and the result is a decrease of the calculated mean emissivty of the substrate (see eq.5). As condensation proceeds, temperature becomes stable and the mean emissivity of the substrate is increasing due to increasing water occupation of the substrate. Both curves S+ and S- increase rapidly until t ≈5000 s due to water droplet condensation. After this time they slowly continue to increase to reach a stable value close to the emissivity of an infinitely thick layer

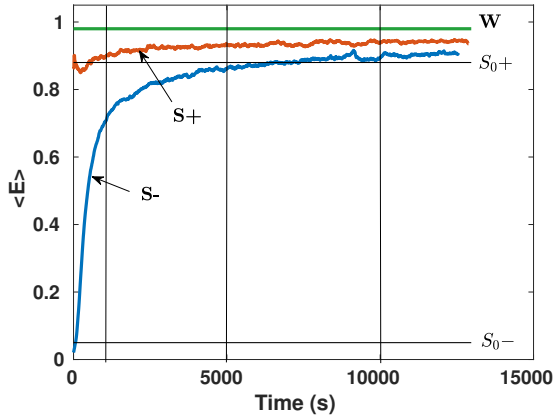

Figure 7: Mean emissivities $< E >$ during condensation corresponding to S+, S- dry substrate. Range : [7.5-14] μm. The vertical lines correspond to the pattern at 1000 s, 5000 s and 10000 s in figure 6 and the horizontal lines So+ and So- to emissivity measured on the dry substrates. W is the effective emissivity of an infinite layer of water corresponding to filmwise condensation. RH=48 %, T_a=26°C, T_c=7.6°C

of water (0.98). Note that S+ reache after about 5000 s its asymptotic value while S- continues to slowly increase. The emissivity of S- anyway remains always smaller than S+, itself lower than the pure water emissivity (W). Finally one can note that the dynamics of S- curve shows a much larger amplitude than curve S+, meaning that the effective emissivity of substrate S- is much more modified by condensation than S+. One will see in the following that the above behavior can be understood in terms of both threshold in droplet size for IR absorption and drop surface coverage evolution.

4.2. Evolution of the condensed mass

When cooling is radiative, the modification of the effective emissivity by droplet condensation influences in turn the condensation dynamics. In order to evidence the effect, two 30 mm disks made of S- and S+ materials are introduced in the radiative chamber. Figure 8 reports the evolution of the condensed mass of water on both substrates. The different curves exhibit similar shape and present two growth regimes: a transient regime characterized by a non-linear

increase of the condensed mass, followed by a permanent regime with constant condensation rate. Both condensation rates in permanent regime are very close with $\dot{m_{S+}}$=3.95×10^{-5} ± 0.05 g.s^{-1} and $\dot{m_{S-}}$=4.13×10^{-5} ± 0.05 g.s^{-1}. However, condensation does not start at the same time for both experiments. In particular, condensation on substrate S- is delayed by Δt ($\approx$ 1000 s) as compared to substrate S+. During this delay, water droplets that have nucleated on substrate defects become large enough to increase the effective emissivity and to ensure an efficient cooling.

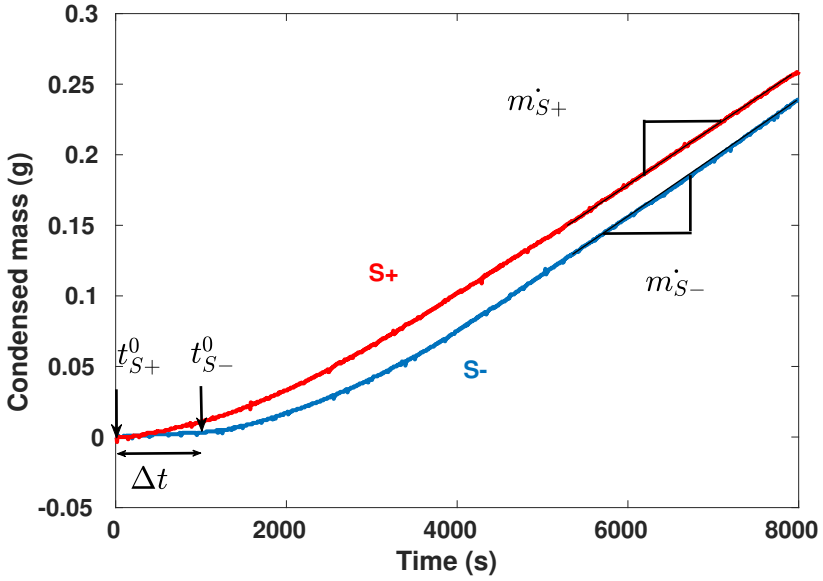

Figure 8: Evolution during radiative cooling of the condensed mass on S+ and S- substrates. T_a=25.1°C, RH=95 %, $\dot{m_{S+}}$=3.95×10^{-5} ± 0.05 g.s^{-1}, $\dot{m_{S-}}$=4.13×10^{-5} ± 0.05 g.s^{-1}

5. Discussions

5.1. Water droplet effective emissivity

In order to understand the difference of behavior between S- and S+ substrates, one needs to determine the radiative properties of each materials. One of the materials is the substrate, whose emissivity and reflectivity are known

and the other is water drops. Thus, we are concerned with the emissivity of spherical caps of water on a substrate.

Transmittivity τ_λ of a water layer with thickness L can be expressed as a function of κ_λ, the spectral absorption coefficient, as:

$$\tau_\lambda = exp(-\kappa_\lambda L) \tag{6}$$

With n_λ the real part and k_λ the imaginary part of the water refractive index ($n^* = n_\lambda + ik_\lambda$) [17],

$$\kappa_\lambda = \frac{4\pi k_\lambda}{\lambda} \tag{7}$$

Note that Equation 6 is only valid for an isothermal, isotropic and homogeneous material, which is considered to be the case for water in this study [REF ?].

The reflection coefficient of the interface air/water in the direction normal to the interface can be expressed as [17]

$$\rho_\lambda = \frac{(n_\lambda - 1)^2 + k_\lambda^2}{(n_\lambda + 1)^2 + k_\lambda^2} \tag{8}$$

Using the refractive index spectral values n_λ and k_λ of water from [18] one can thus deduce the variation with λ of reflectivity ρ_λ (Fig. 9a) and transmittivity τ_λ, the latter for different sample thickness values (Fig. 9b).

Let us now consider a water droplet on a substrate. The drop at the air-water interface partially reflects the radiation from the surrounding environment. Depending on drop thickness, radiation is partly transmitted from the substrate and from the surrounding environment. The radiation trajectory inside a drop is quite complex. Depending on the incidence of radiation, refraction and total reflexion are encountered. In order to treat the problem analytically, the drop is therefore schematized as a cylinder of radius r and height Z_m (figure 10a). In addition, only radiation in the direction normal to the substrate is considered because it is the radiation captured by the camera. L^e is the radiance emitted

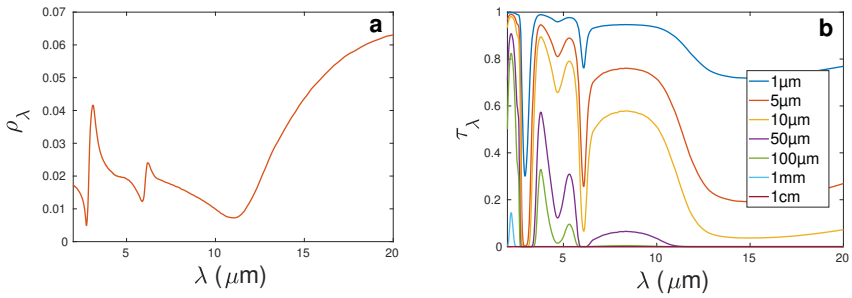

Figure 9: (a) Variation as a function of wavelength λ of ρ_λ, the normal reflection coefficient of the interface air/water. (b): Variation of water transmittivity τ_λ with respect to wavelength λ for different thickness. τ_λ and ρ_λ are calculated from equations 6, 7 and 8 using water optical index values from [18]

by the drop and the substrate and L^i is the radiance coming from the environment. Both are perpendicular to the top of the cylinder thus no refractions are present and the normal radiative properties of water can be used.

The thickness of the cylinder corresponds to the highest point of the drop, that is Z_m, which can be calculated by the following geometric relation where enters the contact angle of the drop on the substrate θ and the effective radius r_e determining the drop view (see Figs. 10ab). For $\theta < 90°$, the drop is approximated by a cylinder of radius $r_e = r$, the radius of contact with the substrate, and height Z_m. For $\theta > 90°$, the drop is approximated by a cylinder of radius $r_e = r/sin\theta$, the drop radius, and height Z_m. Height Z_m can be calculated from geometry as

$$Z_m = r_e(1 - cos\theta) = \frac{r(1 - cos\theta)}{sin\theta} \tag{9}$$

This model obviously oversimplifies the problem because it excludes the angular variability of water emissivity. However it is supported by the relative homogeneity of drops radiations as shown in figure 1. Moreover, Rees and James (1992) [19] show that water angular emissivity only drops for angles higher than 60° which means that only the peripherical region of the drop is concerned with angular emissivity dependance. This region is also concerned

with water transparency due to drop thinning approching the contact line and would require a detailed study to quantify its radiative features.

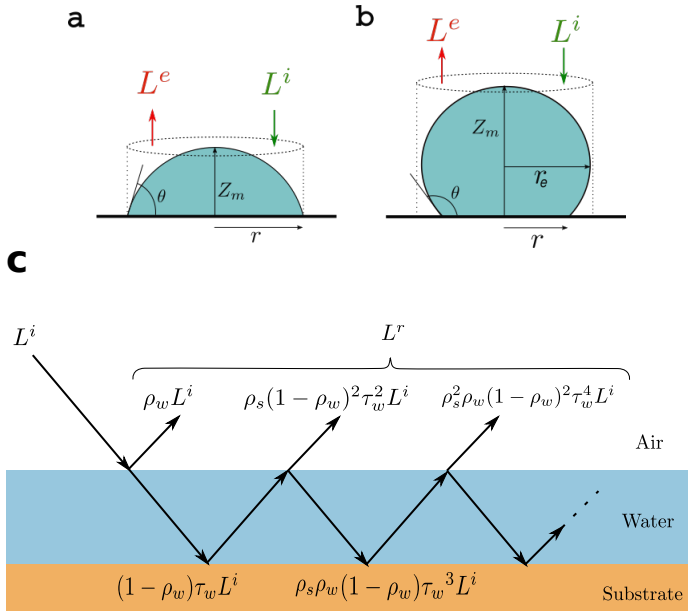

Figure 10: (a) $\theta < 90°$Drop is approximated by a cylinder of radius r and height Z_m. (b) $\theta > 90°$ Drop is approximated by a cylinder of radius r_e and height Z_m. (c) Radiation propagation through a plane layer of liquid water (non-zero incidence angle has been considered for the sake of clarity) The subscript λ has been omitted in order to make the picture more readable.

The effective radiative properties of emission and reflection of a substrate covered with water drops are calculated as follows. Figure 10c shows the trajectory of radiation through the layer of water (radiation is perpendicular to the substrate but an angle is made for the sake of clarity). Radiation L^i_λ corresponds to light incoming at the air/water interface. The fraction $\rho_{\lambda w}$ is reflected while the other fraction $1-\rho_{\lambda w}$ penetrates into water. The fraction $\tau_{\lambda w}$ of the later radiation is transmitted to the substrate, which in turn reflects a fraction $\rho_{\lambda s}$. It follows a sequence of reflections in the substrate and at the water/air interface. Reflected radiance is thus the radiation leaving water after an infinity of successive reflections. From the definition of the reflection coefficient $R_\lambda = L^r_\lambda / L^i_\lambda$

it comes, with k an integer number:

$$R_\lambda = \rho_{\lambda w} + \rho_{\lambda s}(1-\rho_{\lambda w})^2\tau_{\lambda w}^2 \sum_{k=0}^{\infty}(\rho_{\lambda s}\rho_{\lambda w}\tau_{\lambda w}^2)^k \tag{10}$$

This is a geometric serie whose limiting value is

$$R_\lambda = \rho_{\lambda w} + \frac{\rho_{\lambda s}(1-\rho_{\lambda w})^2\tau_{\lambda w}^2}{1-\rho_{\lambda s}\rho_{\lambda w}\tau_{\lambda w}^2} \tag{11}$$

Using Kirchoffs law and the conservation of energy, the effective emissivity of a layer of water on a reflective substrate can be written as $E_\lambda = 1 - R_\lambda$. Note that R_λ being a function of $\tau_{\lambda w}$ and then of the water thickness Z_m (Eq. 6), E_λ and R_λ also depend on Z_m. The integration of the spectral emissivity E_λ between two wavelength $x1$ and $x2$ is made by equation 12 with $L_\lambda^0(T)$ being the spectral radiance of a black body at temperature T.

$$E = \frac{\int_{x1}^{x2} E_\lambda L_\lambda^0(T)d\lambda}{\int_{x1}^{x2} L_\lambda^0(T)d\lambda} \tag{12}$$

In figure 11 is plotted the integration of the emissivity E of a slab of water between two different wavelength ranges as a function of the thickness of the drop for a substrate of low emissivity $\varepsilon_s = 0.05$. The first wavelength range, (I), is [7.5−14] μm corresponding to the atmospheric window and the working range of the IR camera used for the measurements of emissivity. The second range, (II), is $[2 - 50]$ μm and corresponds to the whole range where data were available [18]. As most of the energy of a body at temperature around 10°C is emitted in this wavelength range, the integrated emissivity can be considered as the emissivity at all wavelengths.

It can be clearly seen from figure 11 that there is a thickness threshold Z_m^0 above which the effective emissivity E is constant, with a value equal to the emissivity of a non-transparent material of reflectivity ρ_w. The value is $Z_m^0 \approx 20$ μm for range (I) and effective emissivity stabilizes at $E = 0.98$, while threshold is $Z_m^0 \approx 12$ μm and effective emissivity stabilizes at $E = 0.96$ for range (II). Above Z_m^0 the water transmittivity $\tau_{\lambda w}$ tends to 0, which implies from (11) that

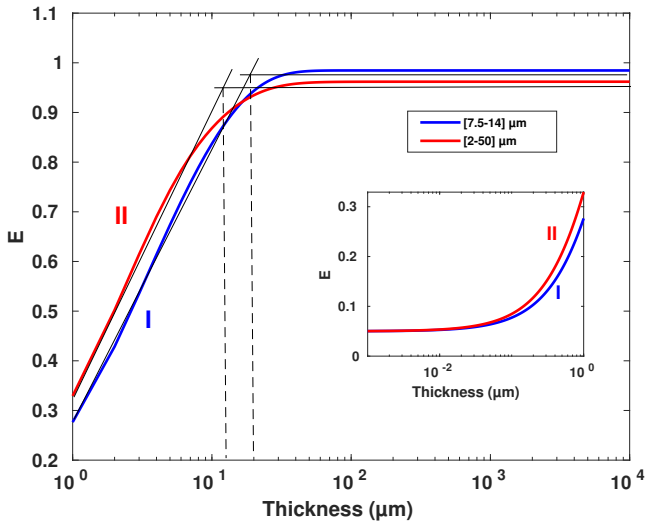

Figure 11: Effective emissivity E for different wavelength range of the assemblage (substrate + drop) as a function of the thickness of the drop (Z_m) (semi-log plot) for substrate S with emissivity $\varepsilon_s = 0.05$. Wavelength ranges (I): $[7.5 - 14]$ μm, (II) : $[2 - 50]$ μm. Vertical lines determine the characteristic length Z_m^0 above which the drop exhibits a constant effective emissivity. Inset: effective emissivities of range (I) and (II) for smaller drop thickness.

the reflection coefficient of the layer of water, R_λ, tends to the reflectivity of the interface air/water $\rho_{\lambda w}$. As $E_\lambda = 1 - R_\lambda$ we get $E_\lambda(Z_m \to \infty) = 1 - \rho_{\lambda w}$. Then, the discrepancy between the effective emissivities for range (I) and (II) can be explained by the spectral distribution of ρ_w in ranges (I) and (II) (figure 9a). Below Z_m^0, the effective emissivity decreases with the drop thickness until reaching a value close to the substrate emissivity (see inset in figure 11.), yet being slighlty higher because of the reflections on the air/water interface.

The above results help to understand the differences of local emissivity from the IR image of drops condensing on a substrate. Figure 1 shows a close up view of condensation on substrate S- (note that experimental conditions are somewhat different from figure 6). Drops with height larger than the threshold Z_m^0 are nearly opaque with large effective emissivity $E = 0.98$ and appear dark (A). As most of the radiance received by the camera come from the emission of

the drops, mean radiance is low. Clearer areas on the IR image (B), with high measured radiance, correspond to the dry substrate revealed because of drop displacement induced by coalescences. The mean radiance of these areas is thus composed of a small contribution from dry substrate emission (low substrate emissivity 0.05) and a large contribution corresponding to the emission of the surrounding environment reflected on the substrate (high substrate reflectivity 0.95). Regions of intermediate radiance (C) and (D) correspond to smaller drops covering the substrate. These drops, not thick enough to be completely opaque, only transmit a fraction of the reflected radiance.

5.2. Mean surface effective emissivity

The surface averaged effective emissivity can be calculated by considering only the completely opaque drops (drops thicker than Z_m^0), the semi-transparent small drops contribution ($Z_m < Z_m^0$) being neglected. What matters is the surface fraction of the projected surface of drops (drop view surface), e_e, calculated from equation 3.

In order to obtain the mean effective emissivity $< E >$ one has to consider the effective emissivity E corresponding to the surface fraction e_e of opaque drops, to which is added the contribution of the dry fraction of the substrate, $1 - e_e$, with emissivity ε_s:

$$< E >= e_e E + (1 - e_e)\varepsilon_s \tag{13}$$

Figure 12 shows the variations of $< E >$ as a function of the contact angle and for different substrate emissivities, as calculated from equations 13, 3 and 1 for $\theta < 90°$. The calculation is made for range (I) ([7.5-14] μm), considering only opaque drops on substrate S-. The effective emissivity of the surface covered by water in equation 13 is thus E=0.98 while the emissivity of the substrate is $\varepsilon_s = 0.05$. In permanent regime, it is commonly observed that at least 3 generations of opaque drops are present. The surface coverage of drops used in equation 13 is thus calculated from equations 2 and 3 with p=3 and e_d^0 coming from equation 1. It evidences that the increase of the contact angle lowers

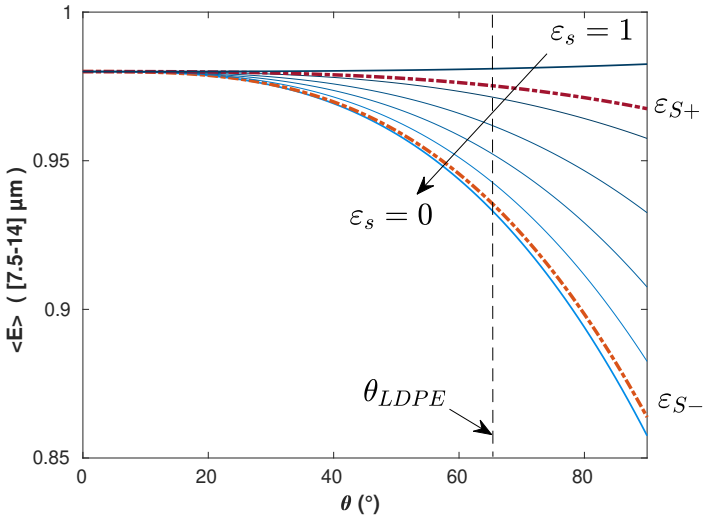

Figure 12: Mean effective emissivity $< E >$ calculated from eq. 13 in the range [7−14] μm, as a function of the contact angle θ and for substrate emissivities ranging from ε_s=1 to ε_s=0. Dotted lines correspond to substrate emissivities of $S+$, ε_{S+} and $S-$, ε_{S-} (see figure 7) while the vertical interrupted line shows values corresponding to the contact angle θ_{LDPE}.

the mean effective emissivity, except for substrate emissivities higher than the emissivity of bulk water. As condensation occurs, e_e approaches unity and the part of the mean effective emissivity due to the substrate emissivity is reduced. This effect explains the evolution of the mean effectivity during condensation (figure 7). At the beginning of the experiment only the dry substrate emissivity is measured. During the first moments of condensation, drops nucleate on substrate defects and start to occupy the surface. But as they are not thick enough to be opaque, the emissivity of the drop on the substrate is still close to the dry substrate emissivity. Then, as drops grow larger, they become less transparent and the substrate effective emissivity increases. Eventually, as the surface coverage stabilizes itself, a pattern appears with opaque large drops, semi-transparent smaller drops and zones clear of condensation, leading to a stabilization of the mean effective emissivity close for all substrates to the high water emissivity. As can be seen on fig. 12. The mean effective emissivity for

substrate S+ and S- ($\varepsilon_{S+} = 0.88$, $\varepsilon_{S-} = 0.05$, $\theta_{LDPE} = 65.9°$) are respectively $< E_{S+} > = 0.975$ and $< E_{S-} > = 0.934$, close to the experimental values in the permanent regime (see figure 7), the discrepancy being due to the transparency of smaller droplets.

5.3. Condensation rate

Figure 8 shows that the dynamics of condensation are similar in both S+ and S- substrates but the delay of condensation is larger on the less emissive substrate S-. In order to understand this dynamics one can consider the following energy balance on the substrate + droplets, supposed to be at the same temperature T [REF?], and thus temperature being uniform on the surface [8].

$$(MC_o + mC_w)\frac{dT}{dt} = \phi_r + \phi_{cv} + \phi_c + \phi_l \tag{14}$$

Here M is the mass of the substrate, with specific heat C_o, and m is water mass, with specific heat C_w. The term $(MC_o + mC_w)dT/dt$ represents the variation of sensible heat of the substrate plus water condensate. ϕ_r represents the net radiative heat flux (difference between absorbed and emitted radiative heat flux), it is negative and corresponds to the cooling power of the system. ϕ_{cv} is the heat flux exchanged by convection with the ambiant air and ϕ_c is heat conduction with the support. Since the substrate is cooler than air during condensation, both are positive. ϕ_l represents the flux of latent heat liberated by condensation to the substrate.

At time $t < 0$ the substrate is dry, there is no condensation and the temperature is stable for both experiment. Thus $dT/dt = 0$ and $\phi_l = 0$. Temperature of the substrate is determined by the balance between the radiative and convective plus conductive heat fluxes, $\phi_r + \phi_{cv} + \phi_c = 0$. The net radiative flux is expressed by

$$\phi_r = \varepsilon S(\phi_i - \sigma T^4) \tag{15}$$

ε is the emissivity of the surface and ϕ_i is the incoming radiative heat flux density. σ is the Stefan-Boltzmann constant. As ϕ_i is fixed, the driving param-

eter of ϕ_r and thus temperature T, is emissivity ε. Low emissivity induces weak radiative cooling flux and large substrate temperature; large emissivity induces high radiative flux and a low subs trate temperature of the substrate. Since $\varepsilon_{S-} < \varepsilon_{S+}$ it thus comes $T_{S-} > T_{S+}$.

The mass balance on water in diffusion limited condensation reads

$$\frac{dm}{dt} = a_w S \left[p_v(T_a) - p_v(T)\right] \approx a_w S \left[p_v(T_a) - p_s(T)\right] \tag{16}$$

The above equation gives the condensation rate dm/dt as a function of the difference in water vapor pressure at substrate temperature T (supposed to be the temperature of water drops), $p_v(T)$ and air temperature at T_a, $p_v(Ta)$. S is the area of condensation and a_w is the water vapor transfer coefficient [8].

At time $t = 0$, humid air enters into the chamber. Since $T_{S-} > T_{S+}$ and thus $p_v(T_{S-}) < p_v(T_{S+})$, according to Eq. 16, the condensation rate dm/dt on S- is lower than on S+ (Fig. 8).

For $t > t^0_{S+}$ and substrate S+ water starts to condense (Fig. 8). After a small diminution due to the temperature drop at the beginning of the experiment coming from the release of latent heat (see sec. 4.1), effective emissivity increases slightly (Fig. 7) due to the growth of water droplets that become opaque to IR. The corresponding increase of emissivity also induces an increase of radiative cooling flux, resulting after about 1000 s to a stationary state.

For $t < t^0_{S-}$ and substrate S- the initial condensation rate is small and the growth of the first condensed droplets is limited. The effective emissivity of the surface as well as the radiative heat flux is not substantially modified by the small drops which are nearly transparent to IR. Thus the temperature of the surface is constant and the condensation rate keeps small, which explains the very low increase of the condensed mass on curve S- in fig. 8. After $\Delta t =$ 1000 s drops reach the threshold size Z^0_m and become opaque to IR radiation. The same dynamic as for substrate S+ occurs with increase of emissivity and cooling radiative flux, leading to the decrease of the surface temperature and the increase of the condensation rate.

In the permanent regime the condensation rates of both experiments are stabilized. As explained in section 4.1 the effective emissivities of both experiments are close to pure water emissivity because of the high surface coverage of opaque drops whose radius is above threshold Z_m^0. It follows that in the steady state regime condensation rates becomes similar and independent on the particular value of the substrate emissivity. The only significant difference between low and high emissivity substrates is the time delay Δt to reach the steady state, larger for low substrate emissivities. Once condensation starts the importance of the substrate emissivity decreases because of the presence of drops with high emissivity. At equilibrium the effective emissivity thus weakly depends on the substrate emissivity and condensation rate becomes independent of the radiative properties of the substrate.

For low substrate emissivity the transient regime however limits condensation yield, because, for same time of condensation, the condensed mass on low emissivity substrates will be smaller than on high emissivity substrates. Moreover, by limiting initially the cooling radiative heat transfer, a low emissive substrate can even prohibit condensation if the threshold in drop thickness Z_m^0 is never reached.

6. Conclusion

In this study we have addressed the contribution of water condensation to the radiative cooling of substrates. Through the lens of what we called the effective emissivity of a condensing surface, we have explored the importance of the emissivity of the base substrate, partially hindered by the presence of condensed droplets which are caracterized by their contact angle on the substrate and their surface coverage ratio. From this study two important results emerge. i) The base substrate emissivity has a major impact at the begining of condensation as it determines the length of a transient regime of condensation when only small drops are present. This transient regime induces a smaller condensation yield for low emissivity substrates. ii) In permanent regime of condensation, the effective

emissivity of a condensing surface is dominated by the presence of drops and the contribution of the base substrate radiative properties in the radiative cooling of the surface is small. The condensation rate in permanent regime is thus nearly independent of the base substrate radiative properties. These results of practical importance can be generalized to any fluid condensation on substate of different emissivity.

Acknowledgements

This work was support by a PhD grant from the French Ministère de l'Enseignement Supérieur et de la Recherche.

References

[1] . Clus, J. Ouazzani, M. Muselli, V. Nikolayev, G. Sharan, D. Beysens, Comparison of various radiation-cooled dew condensers using computational fluid dynamics, Desalination 249 (2009) 707–712.

[2] V. Nikolayev, D. Beysens, A. Gioda, I. Milimouk, E. Katiushin, J.-P. Morel, Water recovery from dew, Hydrology 182 (1996) 19–35.

[3] M. Tomaszkiewicz, M. Abou Najm, D. Beysens, I. Alameddine, M. El-Fadel, Dew as a sustainable non-conventional water resource: a critical review, Environmental Reviews 23 (4) (2015) 425–442. doi:10.1139/er-2015-0035.

[4] T. Nilsson, W. Vargas, G. Niklasson, C. Granqvist, Condensation of water by radiative cooling, Renewable Energy 5 (1-4) (1994) 310–317. doi:10.1016/0960-1481(94)90388-3.

[5] J.-F. Maestro-Valero, V. Martinez-Alvarez, A. Baille, B. Martin-Gorriz, B. Callego-Elvira, Comparative analysis of two polyethylene foil materials for dew harvesting in a semi-arid climate, Journal of Hydrology 410 (2011) 84–91.

[6] J. Trosseille, A. Mongruel, L. Royon, D. Beysens, Radiative cooling for dew condensation, Int. J. Heat and Mass Transfer (under review process).

[7] P. Berdahl, R. Fromberg, The thermal radiance of clear skies, Solar Energy 29 (4) (1982) 299–314.

[8] D. Beysens, Dew Water, River Publishers, Gistrup, 2018.

[9] H. Zhao, D. Beysens, From droplets growth to film growth on a heterogeneous surface, condensation associated with a wettability gradient., Langmuir 11 (1995) 627–634.

[10] D. Beysens, A. Steyer, P. Guenoun, D. Fritter, C. Knobler, How does dew form ?, Phase Transitions 31 (1991) 219–246.

[11] A. ElSherbini, A. Jacobi, Retention forces and contact angles for critical liquid drops on non-horizontal surfaces., Journal of Colloid and Interface Science 299 (2006) 841–849.

[12] A. Al-Mahdouri, M. Baneshi, H. Gonome, J. Okajima, S. Maruyama, Evaluation of optical properties and thermal performances of different greenhouse covering materials, Solar Energy 96 (2013) 21–32.

[13] A. Gustavsen, P. Berdahl, Spectral emissivity of anodized aluminium and the thermal transmittance of aluminium window frames, Nordic Journal of Building Physics 3 (2003) 1–12.

[14] M. Försth, A. Roos, Absorptivity and its dependence on heat source temperature and degree of thermal breakdown., Fire Mater 35 (2011) 285–301.

[15] W. Minkina, D. Klecha, Atmospheric transmission coefficient modelling in the infrared for thermovision measurements, Journal of Sensors and Sensor System 5 (2016) 17–23. doi:10.5194/jsss-5-17-2016.

[16] B. Wiecek, Thermovision in infrared basics and applications (in Polish), Measurement Automation Monitoring Publishing House, 2011.

[17] J. Howell, M. Mengüç, R. Siegel, Thermal Radiation Heat Transfer, CRC Press, 2016.

[18] H. Downing, D. Williams, Optical constant of water in the infrared, J. of Geophysical Research 80 (12) (1975) 1656–1661.

[19] W. Rees, S. James, Angular variation of the infrared emissivity of ice and water surfaces, International Journal of Remote Sensing 13 (15) (1992) 2873–2886. doi:10.1080/01431169208904088.